Full Dimension MIMO for LTE-Advanced and 5G

Young-Han Nam, Md Saifur Rahman, Yang Li,
Gang Xu, Eko Onggosanusi and Jianzhong Zhang
Samsung Research America – Dallas
Richardson, TX 75082, USA
Email: {younghan.n,md.rahman,yang.l,
gary.xu,eko.o,jianzhong.z}@samsung.com

Ji-Yun Seol
Samsung Electronics
Suwon, South Korea
Email: jiyun.seol@samsung.com

***Abstract*—Elevation beamforming and Full Dimension MIMO (FD-MIMO) has been an active area of research and standardization in 3GPP LTE-Advanced. In an FD-MIMO system, a base station with 2-dimensional (2D) active array supports multi-user joint elevation and azimuth beamforming (a.k.a. 3D beamfoming), which results in much higher cell capacity compared to conventional systems. Recent study has shown that with these new FD-MIMO technologies, we can achieve promising 3-5x gain in both cell capacity as well as cell-edge throughput. In this paper, we will provide a brief summary of recent 3GPP activities, including the recently completed 3D channel model, ongoing study on FD-MIMO scenarios, antenna/RF (radio frequency) transceiver architectures, as well as potential network performance benefits. In addition, we also discuss some methods for reducing CSI (channel state information) feedback overhead and ensuring efficient operation of large size FD-MIMO for both TDD and FDD systems.**

I. Introduction

During 3rd generation parternership project (3GPP) long-term-evolution (LTE) Release-12 workshop in 2012, full-dimension multi-input-multi-ouput (FD-MIMO) [1] and user-equipment (UE) specific elevation beamforming were identified as one promising technology to further increase spectral efficiency. In order to facilitate evaluations of FD-MIMO utilizing 2-dimensional (2D) active antenna array, 3GPP had recently completed a study on 3-dimensional (3D) channel models [2]. In October 2014, a new study item on FD-MIMO and UE-specific elevation beamforming [3] was initiated in the 3GPP and industry members have been actively contributing to this study item. It is noted that FD-MIMO is related to massive MIMO [4], [7], [8], [5], [6], in that it also exploits additional degrees of freedom provided by large number of antennas.

This paper will give introduction on newly developed 3D channel models[1] , current development of FD-MIMO scenarios, antenna and RF (radio frequency) transceiver architecutres and potential performance benefits. In addition, challenges related to channel state information (CSI) feedback will be discussed. Candidate methods for reducing CSI feedback overhead will be introduced.

[1]The introductory materials on 3D channel models in this paper have also been reported by authors of the current paper in [9].

II. 3D channel models

3GPP 3D channel models [2] characterize wireless communication channels of typical European cities, in which the building height is distributed with 4 to 8 floors of 3-meters high per floor. With this city model, the height of base station (BS) in UMa scenario is determined to be 25m, and the height of BS in UMi scenario becomes 10m. All outdoor UEs' height is $h = 1.5m$. Indoor UE height is $h = 3(f-1) + 1.5m$, where f is the floor number uniformly distributed within the $[1, N_{floor}]$, in which N_{floor} is uniformly distributed in $[4, 8]$.

A. Antenna Modeling

The 3D channel models support 2D planar (rectangular) antenna array, including cross-pol (x-pol) and co-pol antenna array. In Figure 1, M is the number of rows, and N is the number of columns of the 2D antenna array. For x-pol case, the total number of antenna elements is $2MN$.

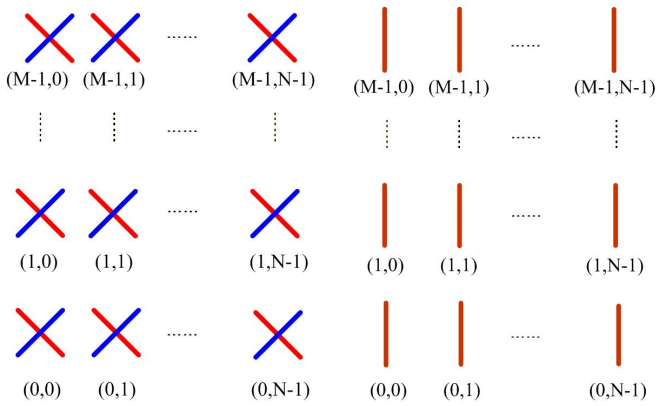

Fig. 1. 2D planar antenna array

Each antenna element has a directional antenna beam pattern, which applies to both azimuth and elevation angles:

$$A''(\theta'', \phi'') = -min\big[-A_{E,V}(\theta'') + A_{E,H}(\phi''), SLA_V\big] \quad (1)$$

where

$$A_{E,V}(\theta'') = -min\Big[-12\Big(\frac{\theta''-90^o}{\theta_{3dB}}\Big)\Big]$$
$$A_{E,H}(\phi'') = -min\Big[-12\Big(\frac{\phi''}{\phi_{3dB}}\Big), A_m\Big] \quad (2)$$

and $\theta_{3dB} = \phi_{3dB} = 65^o$, $SLA_V = A_m = 30$dB, θ'' and ϕ'' respectively are the zenith and the azimuth angles in a base-station antenna coordinate, for which $\phi'' = 0^o$ is azimuth beam broad side, and $\theta'' = 0^o$ is to the zenith.

B. LOS Probability and Pathloss

In LOS cases, pathloss (PL) has traditionally been modeled with a piecewise linear model with two slopes. When Tx-Rx distance is smaller than a break-point (BP) distance, i.e., d_{BP}, the LOS PL decays with a small slope (-2 dB/m) and when the distance is greater, the PL decays with a large slope (-4 dB/m). The BP distance characterizes the distance on which the Fresnel zone [10] is barely broken for the first time. For ground UEs, the effective environment height is $h_E = 1.0m$, the BP distance d_{BP} is:

$$d_{BP} = 4(h_{BS} - h_E)(h_{UE} - h_E)f_c/c, \quad (3)$$

where h_{BS}, h_{UE}, f_c, and c are respectively BS height, UE height, carrier frequency, and speed of light. For high-floor UEs two different types of LOS can be defined. In one type (denoted as Type 1), the LOS link is over the street; in another type (denoted as Type 2), the LOS link is over buildings. These different types of LOS changes h_E, d'_{BP}, and finally the LOS PL. For UEs on 5th or higher floor, the LOS type is stochastically determined, and these parameters and LOS PL are correspondingly to be calculated. It is noted that the BP distance of LOS Type 2 is shorter than that of LOS Type 1 because the Fresnel zone breaks earlier owing to the higher environment height.

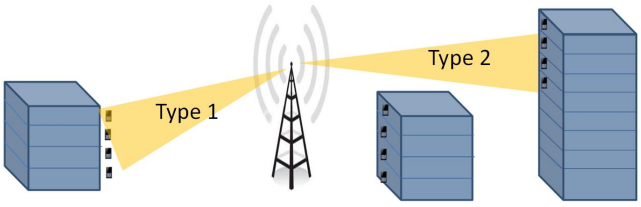

Fig. 2. LoS types

In NLOS cases, for indoor UEs, PL is determined as a function of UE height, and the PL gets smaller as for higher UE due to over-the-rooftop diffraction as illustrated in Figure 3. Higher-floor UEs have smaller diffraction angles, and hence the PL becomes smaller. This over-the-rooftop diffraction effect is more prominent in UMa scenario than UMi scenario, as the main propagation mechanism in UMa is over-the-rooftop diffraction and the one in UMi is around-the-building diffraction that incurs little height path gain. The different height-gain scaling factors are captured:

$$PL_{3D-UMa}(d, h_{UT}) = PL_{2D-UMa}(d) - 0.6(h_{UE} - 1.5),$$
$$PL_{3D-UMi}(d, h_{UT}) = PL_{2D-UMi}(d) - 0.3(h_{UE} - 1.5) \quad (4)$$

where $PL_{2D-UMa}(d)$ and $PL_{2D-UMi}(d)$ respectively correspond to PL in legacy (i.e., 2D) channel models in the UMi and the UMa scenarios.

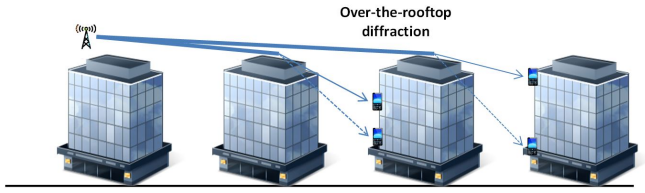

Fig. 3. NLoS pathloss

C. Fast Fading Models

In spatial channel models, channel response is a composite of multi-path clusters to Tx/Rx antennas. Each cluster is characterized by power, delay, phase, angle of arrivals and angle of departures of N clusters. When x-pol is also modeled, the channel response of an Rx antenna u, a Tx antenna s, and a path (or cluster) n is represented by:

$$H_{u,s,n} = \sqrt{\frac{P_n}{M}} \sum_{m=1}^{M} \begin{bmatrix} F_{rx,u,\theta} \\ F_{rx,u,\phi} \end{bmatrix}^T \begin{bmatrix} exp(j\Phi_{n,m}^{\theta,\theta}) & \sqrt{\kappa_{n,m}^{-1}} exp(j\Phi_{n,m}^{\theta,\phi} \\ \sqrt{\kappa_{n,m}^{-1}} exp(j\Phi_{n,m}^{\phi,\theta}) & exp(j\Phi_{n,m}^{\phi,\phi} \end{bmatrix} \cdot \begin{bmatrix} F_{tx,s,\theta} \\ F_{tx,s,\phi} \end{bmatrix} exp(j2\pi v_{n,m} t) \cdot \exp\left(j2\pi\lambda_0^{-1}\hat{r}_{rx,n,m}^T \bar{d}_{rx,u}\right) exp\left(j2\pi\lambda_0^{-1}\hat{r}_{tx,n,m}^T \bar{d}_{rx,u}\right). \quad (5)$$

Here, $F_{rx,u,\theta}$ and $F_{rx,u,\phi}$ (and $F_{tx,s,\theta}$ and $F_{tx,s,\phi}$) respectively are field patterns of Rx antenna u (and Tx antenna s). The 2x2 matrix between the arrival and departure field pattern vectors is the depolarization matrix, of which two diagonal elements characterize the co-polarized phase response, and the two off-diagonal elements model the cross-polarized phase response and power attenuation $\sqrt{\kappa_{n,m}^{-1}}$. Here $\hat{r}_{rx,n,m}$ is the spherical unit vector with azimuth arrival angle $\phi_{n,m,AOA}$ and zenith arrival angle $\theta_{n,m,ZOA}$, given by:

$$\hat{r}_{rx,n,m} = \begin{bmatrix} sin\left(\theta_{n,m,ZOA}\right) cos\left(\phi_{n,m,AOA}\right) \\ sin\left(\theta_{n,m,ZOA}\right) sin\left(\phi_{n,m,AOA}\right) \\ cos\left(\theta_{n,m,ZOA}\right) \end{bmatrix} \quad (6)$$

and $\hat{r}_{tx,n,m}$ is the spherical unit vector with departure angles and is similarly defined. $\bar{d}_{rx,u}$ and $\bar{d}_{tx,u}$ are respectively the location vectors of receive antenna element u and transmit antenna element s. λ_0 is the wavelength of the carrier frequency.

Comparing this equation with the counterpart in legacy channel models, the major difference is the newly introduced elevation (or zenith) angle parameters: $\theta_{n,m,ZOA}$ and

$\theta_{n,m,ZOD}$. If zenith angle distribution is rich, there will be more chances to apply MU-MIMO along zenith angles.

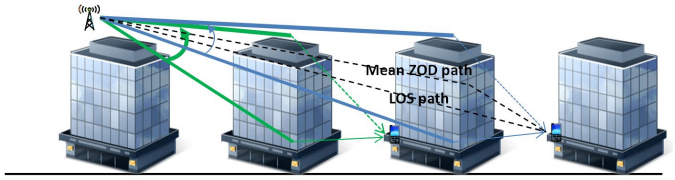

Fig. 4. Illustration of elevation angles

As shown in Figure 4, when over-the-rooftop diffraction is dominant propagation mechanism (e.g., UMa), the zenith angle distribution is not centered around the zenith LOS angle but with a small offset. Furthermore, this offset decreases with distance, because a far-away cell from a UE tends to have zenith angle, regardless of whether the corresponding link is LOS or not. In addition, the zenith angle spread also decreases in distance. Finally, these height dependent ZOD parameters depend on outdoor links condition. The mean angle offset applies only if outdoor link condition is NLOS but not LOS.

III. Recent 3GPP development of FD-MIMO

As of January 2015, 3GPP had two meetings on FD-MIMO, and had major progress on the transceiver architecture. The 3GPP has also published a first version of technical report on FD-MIMO [11].

In FD-MIMO architecture reflecting typical implementation of 2D active antenna systems, MIMO precoding of a data stream goes through three stages: (1) *antenna-port virtualization*: a stream on an antenna port is precoded on T_1 transceiver units (TXRUs); (2) *TXRU virtualization*: a signal on a TXRU is precoded on T_2 antenna elements; and (3) *antenna element pattern*: a signal emitted from an antenna element will have a directional gain pattern. It is noted that in traditional transceiver architecture modeling, a static one-to-one mapping is assumed between antenna ports and TXRUs, and TXRU virtualization effect is combined into a static (TXRU) antenna pattern which captures both effects of TXRU virtualization and antenna element pattern.

Antenna port virtualization is an operation in the digital domain, and it refers to digital precoding that can be performed in frequency-selective manner. In LTE, an antenna port is defined in conjunction with a pilot, or a reference signal. For example, for precoded data transmission on an antenna port, demodulation reference signal (DMRS) is transmitted on the same bandwidth as the data signals, and both DMRS and data are precoded with the same digital precoder (or with the same TXRU virtualization precoding). For CSI estimation, on the other hand, CSI reference signal (CSI-RS) are transmitted on multiple antenna ports. For CSI-RS transmissions, the precoder characterizing the mapping between CSI-RS ports to TXRUs can be designed as an identity matrix, to facilitate mobile's estimation of TXRU virtualization precoding matrix for data precoding vectors.

TXRU virtualization is an analog operation, and hence it refers to time-domain analog precoding. TXRU virtualization can be made time-adaptive. When TXRU virtualization is semi-static (or rate of change in TXRU virtualization is slow, e.g., slower than in an order of seconds), TXRU virtualization weights of a serving cell can be chosen to provide good coverage to its serving mobiles and to reduce interference to other cells. More challenges are anticipated if TXRU virtualization is dynamic (or the rate of change is fast, e.g., in an order of milli-seconds), in terms of hardware implementation and protocol design, yet more study seems to be necessary whether or not performance gain can justify expenditure to resolve these challenges.

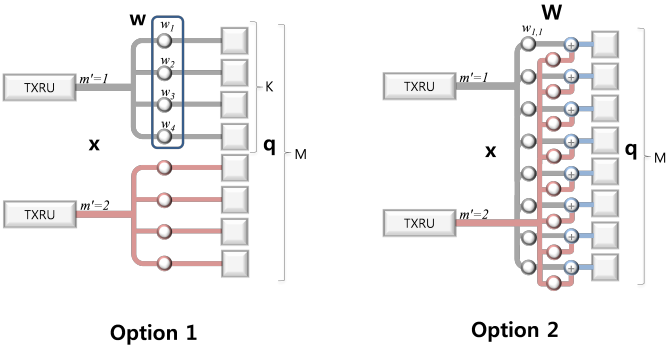

Fig. 5. 1D TXRU virtualization: Option 1 for subarray partition; Option 2 for full-connection

Two TXRU virtualization methods are agreed for further study: (1) *1D TXRU virtualization*; and (2) *2D TXRU virtualization*. In 1D TXRU virtualization, M_{TXRU} TXRUs are associated with only those M antenna elements comprising a column antenna array with the same polarization. With N columns in the 2D antenna array and dual-polarized configuration ($P = 2$), the total number of TXRUs in this case is $Q = M_{\mathrm{TXRU}} \cdot N \cdot P$. In 2D TXRU virtualization, Q TXRUs can be associated with any of MNP antenna elements. It is expected that these two different TXRU architectures will have different tradeoffs, in terms of hardware complexity, power efficiency, hardware cost and performance, and further discussion will take place in the future 3GPP meetings.

For each method, two architectures are being considered: (a) *subarray partition*; and (2) *full-connection*. In subarray partition, antenna elements are partitioned into multiple groups of same number of elements. In 1D subarray partition, M antenna elements comprising a column are partitioned into groups of K elements. In 2D subarray partition, $N_t = MNP$ antenna elements are partitioned into rectangular array of $K_1 \times K_2$ elements. On the other hand, in 1D full connection, a signal output of each TXRU associated with a column antenna array with a same polarization is split into M signals, and those M signals are precoded by a group of M phase shifters or variable gain amplifiers. Then, M_{TXRU} weighted signals are combined at each antenna element. In 2D full connection, a signal output of each TXRU is split into MNP signals,

and those MNP signals are precoded by a group of MNP phase shifters or variable gain amplifiers. Then, Q weighted signals are combined at each antenna element. An illustration of 1D subarray partition and full connection architectures can be found in Figure 5.

Antenna element pattern is typically designed to provide horizontal sectorization coverage. For example, to have a 3-sector coverage, each antenna element is designed to have 65 degree horizontal 3dB beam width. In 3GPP antenna element pattern, vertical beam width is also 65 degree. With an antenna configuration of $M = 8$ and vertical spacing of $d_V = 0.8\lambda$ and applying DFT weights on those 8 antenna elements, the resulting elevation beam width is about 10 degrees. With an application of about 10 degree elevation steering, this configuration establishes a null at 90 degree zenith angle, which can greatly reduce interference to far-away cells.

IV. CSI Feedback for FD-MIMO

In recent 3GPP meetings, various CSI feedback schemes have been discussed. Some of these schemes are standard-transparent and developed based on Release 12 specifications, while the rest are standard-enhancement schemes. Among them, the Kronecker-product (KP) based CSI framework designed for the subarray architecture is considered by many companies and appears to be a promising solution to practically achieve gains expected from the FD-MIMO systems. Therefore, this paper focuses on KP based schemes.

A. KP-Based CSI Framework

The KP-based CSI framework relies on the assumption that the 3D channel $\mathbf{H}_{3D}$ between an eNB and a UE can be approximated by the Kronecker-product between the azimuth and elevation domain channels $\mathbf{H}_h$ and $\mathbf{H}_v$, respectively, i.e.

$$\mathbf{H}_{3D} \approx \hat{\mathbf{H}}_{3D} = \mathbf{H}_h \otimes \mathbf{H}_v. \tag{7}$$

Let $\mathbf{w}_{3D} = \mathbf{w}_h \otimes \mathbf{w}_v$ be a KP pre-coder, where $\mathbf{w}_h$ and $\mathbf{w}_v$ are the azimuth and elevation domain pre-coding vectors, respectively. We have the following commuting property of KP:

$$\hat{\mathbf{H}}_{3D}\mathbf{w}_{3D} = (\mathbf{H}_h \otimes \mathbf{H}_v)(\mathbf{w}_h \otimes \mathbf{w}_v) \tag{8}$$

$$= (\mathbf{H}_h\mathbf{w}_h) \otimes (\mathbf{H}_v\mathbf{w}_v). \tag{9}$$

Therefore, the overall PMI pre-coder computation can be decoupled into two separate PMI pre-coder computation for the two dimensions based on the respective channels if we consider KP-based overall PMI pre-coder. However, the remaining two CSI components, CQI and RI, also need to be computed by the UE in order to complete the CSI report to be sent to the eNB. Depending on whether the CSI components are computed independently based on the azimuth and elevation domain channels or jointly based on the full channel, KP-based CSI feedback schemes can be differently defined. Two candidate KP-based schemes that are currently considered by the industry are summarized next.

1) Transparent KP-Based CSI Feedback Scheme: In a standard-transparent KP-based CSI scheme, a UE is configured with 2 CSI processes, H-CSI and V-CSI processes. CSI processes are originally introduced for facilitating CSI feedback for coordinated multipoint (CoMP) transmission [13], the feature of which allows CSI feedbacks with different assumptions, and the 2 CSI processes can be used in FD-MIMO systems, not requiring to change standards specifications. On the H-CSI process CSI constitutes H-PMI, H-CQI, and H-RI, which are computed for the azimuth domain channels. Similarly, on the V-CSI process CSI constitutes V-PMI, V-CQI, and V-RI, which are computed for the elevation domain channels. Based on the two CSI configurations, the UE computes the two CSI reports and feeds them back to the eNB. The eNB uses the two reports to reconstruct the 3D CSI components as follows:

1) a composite PMI pre-coder is the KP of the two PMI precoders: H-PMI and V-PMI pre-coders,
2) a CQI is the product of the two CQI, i.e. $CQI_{3D} = H-CQI \times V-CQI$, and
3) a RI is the maximum of the two reported ranks, H-RI and V-RI.

2) Enhanced KP-Based CSI Feedback Scheme: In a standard-enhancement KP-based CSI scheme, a UE is configured with 1 or 2 CSI processes. The CSI constitutes two PMIs, H-PMI and V-PMI for the azimuth and elevation domain channels, respectively, a joint CQI (J-CQI) based on the full channel, and a joint RI (J-RI) corresponding to the J-CQI. Based on the CSI configuration, the UE computes and reports the CSI to the eNB.

3) Discussions on the KP-Based CSI Feedback Schemes: Enhanced KP is expected to give more performance benefits than transparent KP. In figure (6), system level simulation results in terms of cell-average throughput are shown for the KP-based CSI schemes for a system in which the eNB has an $8H \times 4V$ antenna configuration. For comparison, the results for $(8H \times 1V)$ baseline and ideal CSI schemes are also provided. In these results, LTE 8-Tx codebook and LTE 4-Tx codebooks are considered for H-PMI and V-PMI pre-coding vectors, respectively. As shown, there is about 20 percent additional gain with the enhanced KP based CSI scheme compared to the transparent KP-based CSI scheme. However, compared to the ideal CSI scheme, in which ideal CSI is available at the eNB, the enhanced KP-based CSI scheme results in much worse performance. One possible reason of this gap is that the KP of the legacy codebooks may not give sufficient precision in quantizing the 3D channels. In particular, in case 8-Tx codebook, the wideband W1 codebook consisting of basis sets of four oversampled DFT beams may not be optimal wideband basis for the wideband quantization of 3D channel, and the subband basis coefficients for the four beams in terms of beam selection and co-phasing by the W2 codebook may not be the optimal basis coefficients.

4) Linear combination PMI codebook: As one solution to reduce the performance gap between ideal CSI and codebook based approach, we propose a novel scheme in which the

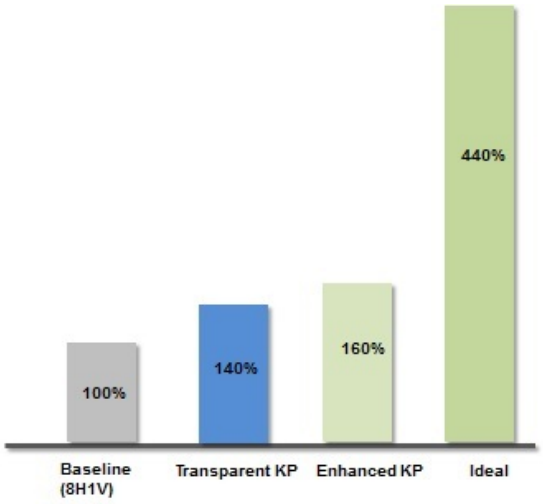

Fig. 6. Cell-average throughput

PMI codebook consists of a master basis set and coefficients. This is an extended work from our previous work in [12], which has proposed an explicit channel feedback. Departing from the channel feedback in our previous work, this paper proposes to use precoder feedback. In this framework, PMI feedback from the UE consists of a wideband basis set index and subband coefficients. Since the AoD spread of the 3D channels is expected to be small and antenna array aperture is limited, the dominant eigenvector $\mathbf{h}$ of the channel $\mathbf{H}_{3D}$ can be represented as a linear combination of basis set consisting of DFT beams $\{\mathbf{B}_{k,l}\}$:

$$\mathbf{h} \cong \sum_{(k,l)\in\Gamma} c_{k,l}\mathbf{B}_{k,l},$$

where Γ denotes the set of indices associated with the subset of phase values capturing the multi-path components of a link, and $c_{k,l}$ and $\mathbf{B}_{k,l}$ respectively are the channel coefficient and the DFT basis vector associated with the index pair (k,l).

In the proposed CSI feedback scheme, the UE estimates the DL channel states using CSI-RS. Once the DL channel channel states are estimated the UE first selects a wideband basis set of a fixed size according to the CSI configuration, and then computes the subband coefficients based on coefficient codebook. The basis set combination and the corresponding coefficients are then fed back to the eNB.

5) Performance Evaluation: Figure 7 shows the capacity based performance evaluation of the proposed CSI feedback scheme. In the figure, the sum-rate capacity of the two user MU-MIMO with SLNR pre-coding and MMSE-IRC receiver at the two UEs is shown. The ideal (subband) eigenvector feedback plot is provided as an outer bound. Release 12 based 16-Tx codebook based CSI scheme is considered as an inner bound. 8-Tx baseline ($8H \times 1V$) result is also provided for comparison. For the proposed scheme, the results for subset set sizes 6 and 8 with and without subband coefficient quantization are shown. The optimal wideband basis set is first obtained out of the all candidate basis sets, and then

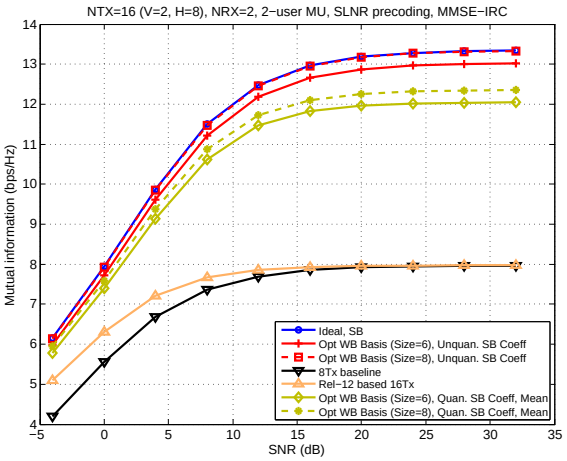

Fig. 7. Sum-rate capacity vs. SNR: two-user MU-MIMO

mean of the quantized coefficients is computed using the coefficient codebook. For coefficient codebook, Lloyd-based vector quantization is employed where the size of the vector is 48 (number of subcarriers in a subband). The real and the imaginary parts of the coefficients are separately quantized using the same codebook. The size of the codebook is 32; therefore, 5 bits per real coefficient or 10 bits per complex coefficient is assumed.

It is evident from the capacity based analysis that the proposed CSI feedback scheme can achieve much improved performance compared to the Release 12 based 16-Tx codebook based CSI scheme. Also, the performance can be improved further by considering a larger basis set.

V. Conclusion

This paper has reviewed recent development of FD-MIMO in 3GPP LTE and presented a novel CSI feedback method. 3D channel models developed for FD-MIMO system level analysis have been introduced and summarized, and FD-MIMO system architecture being studied in 3GPP has been reviewed. In addition, challenges related to FD-MIMO CSI feedback have been discussed, and system-level performance of transparent and enhanced KP based CSI feedback methods has been compared against ideal CSI feedback. It has been observed that KP based CSI feedback schemes have limitation achieving

ultimate FD-MIMO performance in their current forms, and an alternative solution, linear combination codebook has been proposed. The preliminary capacity analysis results has shown that the linear combination codebok has a good potential to improve the FD-MIMO performance in FDD systems.

REFERENCES

[1] Y. H. Nam, B. L. Ng, K. Sayana, Y. Li, J. Zhang, Y. Kim and J. Lee, "Full-dimension MIMO (FD-MIMO) for next generation cellular technology," IEEE Communications Magazine, Vol. 51, Issue 6, Jun. 2013.

[2] 3GPP TR 36.873, "Study on 3D channel model for LTE," September 2014

[3] RP-141644, "New SID proposal: study on elevation beamforming/full-Dimension (FD) MIMO for LTE," Samsung, Nokia Networks, 2014.

[4] T. L. Marzetta, "Noncooperative cellular wireless with unlimited numbers of base station antennas", IEEE Trans. Wireless Communications, vol. 9, no. 11, pp. 3590-3600, Nov 2010.

[5] E. Larsson, O. Edfors, F. Tufvesson, T. Marzetta, "Massive MIMO for next generation wireless systems," IEEE Comm. Mag., Feb. 2014

[6] L. Lu, G. Y. Li, A. L. Swindlehurst, A. Ashikhmin, R. Zhang, "An overview of massive MIMO: benefits and challenges," IEEE JSAC, Oct. 2014

[7] F. Boccardi, R. W. Heath, Jr., A. Lozano, T. L. Marzetta, and P. Popovski, "Five disruptive technology directions for 5G," IEEE Communications Magazine, vol. 52, no. 2, pp. 74-80, Feb. 2014.

[8] K. T. Truong and R. W. Heath, Jr., "Effects of channel aging in massive MIMO systems," Journal of Communications and Networks, Special Issue on Massive MIMO, vol. 15, no. 4, pp. 338-351, August 2013.

[9] Y. H. Nam, Y. Li and J. Zhang, "3D channel models for elevation beamforming and FD-MIMO in LTE-A and 5G," Asilomar Conference on Signals, Systems and Computers, November 2014.

[10] H. Masuri, et al., "Microwave path-loss modeling in urban line-of-sight environments," IEEE Trans. Selected Area in comm., 2002.

[11] 3GPP TR 36.897 v0.1.1, "Study on elevation beamforming/full-dimension (FD) MIMO for LTE," November 2014.

[12] E. Onggosanusi, Y. Li, M. S. Rahman, Y. H. Nam, J. Zhang, J. Y. Seol and T. Y. Kim, "Reduced space channel feedback for FD-MIMO," IEEE International Conf. on Comm, 2015 (accepted).

[13] J. Lee, et. al., "Coordinated multipoint transmission and reception in LTE-Advanced systems," IEEE Communications Magazine, Nov. 2012.